

TEXTURE EVOLUTION DURING COMPRESSION IN ZIRCALOY-2

F. Xu, R.A. Holt, D. Durance and M.R. Daymond
Queen's University, Kingston, Ontario K7L 3N6, Canada

Abstract

The deformation of Zircaloy-2 is influenced by many factors; one being bulk texture. The texture can greatly affect the development of both the macro-mechanical (e.g. stress-strain curve) and micro-mechanical behavior (e.g. intergranular stresses). Thus studies on texture evolution are of practical significance. This introduces our current work on texture development during uniaxial loading of warm rolled Zircaloy-2 slab. As manufactured, most basal poles are orientated along the normal direction (ND), with a spread of $\pm 50^\circ$ towards the transverse direction (TD) and $\pm 30^\circ$ towards the rolling direction (RD). The $\{11\bar{2}0\}$ normals are moderately concentrated in RD. Compression tests were performed in-situ during neutron diffraction to follow the development of lattice strain and intensity for eight diffraction peaks, with two tests each for compression along ND, TD and RD. Pole figures were then measured for the deformed samples. In this paper, we report the results for compression along RD. The development of intensity measured in two perpendicular directions during compression along RD showed that tensile twinning occurred during the deformation, which was confirmed by the subsequent texture measurement. Modeling work was performed with a visco-plastic self-consistent model (VPSC), assuming that prism $\langle a \rangle$ slip, basal $\langle a \rangle$ slip, pyramidal $\langle c+a \rangle$ slip and tensile twinning are the active deformation mechanisms. The model successfully reproduced the macroscopic stress-strain responses, and also predicted the final texture reasonably well. Although further work is needed to refine the results, the model predicts reasonably well tensile twinning activity, and the twinning-induced reorientation of basal poles from ND to RD, and prism poles from RD to ND.

Keywords: Intensity, Texture, Neutron diffraction, VPSC, Zircaloy-2

1. Introduction

Zircaloy-2 (Zr, 1.20-1.70 wt% Sn, 0.07-0.2 wt% Fe, 0.05-0.15 wt% Cr, 0.03-0.08 wt% Ni, 900-1400 ppm O) [1] has a stable α -phase (*hcp*) below 1156K and exhibits anisotropy in the thermal, elastic and plastic properties, both at the single crystal and polycrystal levels. The material is widely used in nuclear reactors due to its low neutron capture cross-section, excellent corrosion-resistant properties, and reasonable mechanical properties. In CANDU reactors, this material is used for the calandria tubes. Excessive deformation during operation in the irradiation environment of the reactor may lead to serious problems, such as the pressure tube-to-calandria tube contact [2]. The deformation is closely related to the development of intergranular stresses (Type-2 Stresses), i.e. the stresses developed between different grain orientations during manufacturing. It is necessary to understand the development of Type-2 stresses in order to predict the behavior of a material made by a new manufacturing route, for example the calandria tubes for the Advanced CANDU Reactor [3].

There are many factors that can influence the accumulation of Type-2 stresses: one of the most important factors is bulk texture. The texture in Zircaloy-2 polycrystals usually develops during manufacturing, such as rolling or extrusion, and results in anisotropic properties in the final product. The texture is a combined result of anisotropic single crystal properties, grain interactions and the external loading.

Plastic deformation at room temperature in Zircaloy-2 is usually accommodated by prism $\langle a \rangle$ slip $\{10\bar{1}0\}\langle 11\bar{2}0 \rangle$, tensile twinning $\{10\bar{1}2\}\langle 10\bar{1}1 \rangle$, pyramidal $\langle c+a \rangle$ slip $\{10\bar{1}1\}\langle 11\bar{2}3 \rangle$, and compressive twinning $\{11\bar{2}2\}\langle 11\bar{2}3 \rangle$, in order of ease of activation. There is still some debate

about the presence of basal $\langle a \rangle$ slip $\{0001\}\langle 11\bar{2}0 \rangle$ at room temperature [4,5], but it appears to be necessary to model the behavior [6]. Relating the activation of various deformation modes to texture evolutions, Ballinger et al. [7,8] found (for a similar texture to that used in our study) that: (1) prism slip accounts for most of the large axial expansions or contractions and rotates the $\{10\bar{1}0\}$ planes into the rolling direction (RD) during tension along RD; (2) compressive strains achieved through pyramidal slip will rotate the $\{10\bar{1}1\}$ plane such that it will approach the normal to the compression axis; (3) pyramidal slip can also create a spread of basal poles peaked in the normal-transverse (ND-TD) plane at approximately $30\text{-}40^\circ$ to TD; and (4) twinning rotates grains into an orientation favorable for prism slip which makes accommodation of strains in other grains easier. Hobson et al. [9] suggests that twinning is more important in the initial stages and that slip is more important in the final stages of texture development, thus the occurrence of twinning (especially tensile twinning) has received much attention in our studies. The activation of tensile twinning involves a reorientation of 85.22° of the basal and prism poles, resulting in basal pole orientation $\sim 90^\circ$ away from ND during tension along ND, Figure 1 [10].

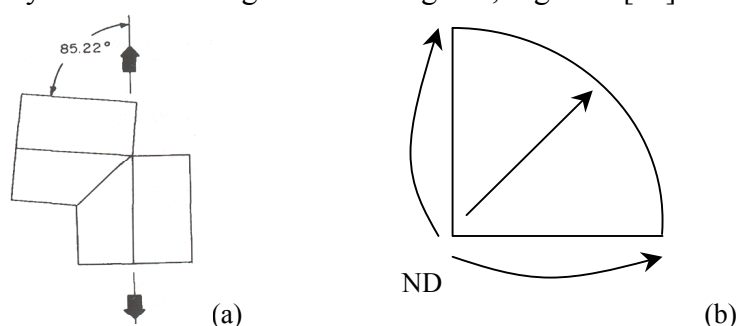


Figure 1. Tensile twinning in α -zirconium indicating the reorientation of the hcp structure and for tension along ND (where most of the basal plane normals are concentrated), rotation of the basal plane normals to the periphery of the pole figure [10]

The development of texture is generally understood experimentally. However, there has been limited success in modeling it. Part of the reason is due to the limited understanding of twinning and hardening (e.g. how multiple deformation systems interact with each other). The theory for the texture simulation of noncubic crystals is well behind that of cubic crystals [11], due to the more restricted availability of slip the greater possibilities of twinning. Also there are other issues remain to be understood: e.g. the impact of the initial texture (associated with previous deformation), the impact of texture development on the intergranular stresses and the impact of more complicated stress states and loading than simple uniaxial ones.

Currently, we are investigating the evolution of lattice strain and texture in Zircaloy-2 by neutron diffraction (time-of-flight) during *in-situ* uniaxial compression along three principal directions. The development of three-dimensional lattice strains for both compression and tension along three directions has been reported in Ref. [12]. Some intensity changes were included in Ref. [13]. In this paper, we revisit some of the intensity changes and report the measured final texture, for compression along RD. In particular, we emphasize the role of tensile twinning, and its effects on the texture evolution. A visco-plastic self-consistent model (VPSC) is used to predict the final texture, and to illustrate how slip and tensile twinning contribute to this texture.

2. Experimental Procedure

The source material is a warm-worked Zircaloy-2 slab, 60mm thick with most of the basal poles orientated near ND, with a spread of $\pm 50^\circ$ towards TD and $\pm 30^\circ$ towards RD [14]. The $\{11\bar{2}0\}$ normals are moderately concentrated in RD. The manufacturing process of the slab was not well documented but it appears to have recrystallized, inducing a 30° rotation of the texture about the basal pole, rotating the $\langle 11\bar{2}0 \rangle$, rather than the $\langle 10\bar{1}0 \rangle$ direction into RD [7, 14].

Six samples for the compression tests were machined from the slab at the middle thickness (to ensure the uniform texture throughout the sample) in the three principal directions, with two samples each being prepared for compression along ND, along RD and along TD. Each sample was machined to a right circular cylinder, with 9mm in diameter and 18mm in height. *In-situ* compression tests were performed on the ENGIN-X beam line at the ISIS facility, Rutherford Appleton Labs. (UK). Experimental details have been given in Ref. [13]. The loading axis is set horizontally at 45° to the incident beam so that it is possible to measure lattice strains in directions both parallel and perpendicular to the axis in two detector banks which are aligned horizontally at scattering angles of $\pm 90^\circ$. Figure 2 shows a schematic experimental set-up for the sample tested in ND. Intensities and lattice strains in RD and ND (Figure 2b) (or TD and ND, Figure 2c) can be measured simultaneously using Detector 1 and 2, respectively. Four compression tests were performed over -12% strain, while one sample compressed in RD was stopped earlier at $\sim 8\%$ strain and one for ND at $\sim 5\%$ strain, due to the time constraints. The measured diffraction peaks are $\{10\bar{1}0\}$, $\{0002\}$, $\{10\bar{1}1\}$, $\{10\bar{1}2\}$, $\{11\bar{2}0\}$, $\{10\bar{1}3\}$, $\{20\bar{2}0\}$, $\{11\bar{2}2\}$, $\{20\bar{2}1\}$, $\{0004\}$, and $\{20\bar{2}2\}$, in order of high to low inter-planar spacing. Peak intensities were obtained by fitting the recorded spectra with Gaussian function using GSAS rawplot [15].

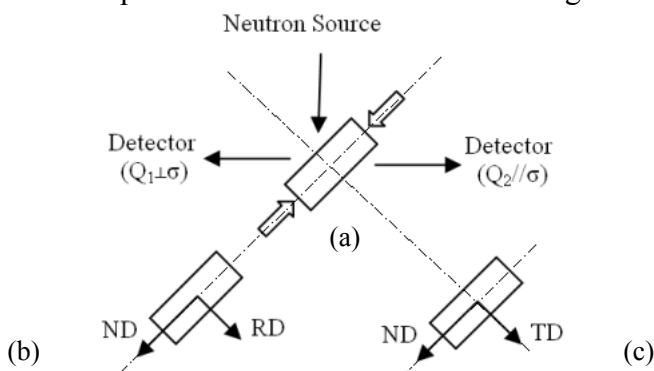


Figure 2. Sample positioning for compression tests along ND, (a). The sample can be tested such that (b) $Q_1 \parallel RD$ and $Q_2 \parallel ND$ or (c) $Q_1 \parallel TD$ and $Q_2 \parallel ND$.

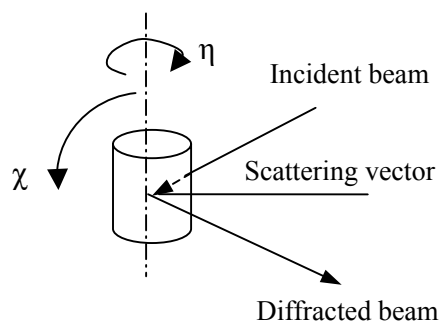


Figure 3. Definition of η and χ

Textures of the samples after compression were measured at the NRU reactor, Chalk River Labs., using the constant-wavelength neutron diffraction technique on the E3 triple-axis spectrometer. The deformed sample was positioned on the goniometer with its compression axis being normal to the plate of the sample holder table. Samples were measured, each having been compressed to more than -12% strain along ND, TD or RD. The intensity of three diffraction peaks was measured in 5° increments over the complete hemisphere defined by the polar angle η and the azimuthal angle χ of the goniometer relative to the compression axis of the specimen (η from 0° to 360° and χ from 0° to 90° , Figure 4). In order to obtain the maximum counting statistics of neutron diffraction, the whole sample was bathed in the incident beam. Therefore background intensity was also measured over the complete hemisphere to correct the diffracted intensities for anisotropic absorption due to the non-spherical shape of the sample. The measured textures for the samples compressed along RD and TD were rotated such that the center of all the pole figures is ND, and the north pole is RD.

3. Self-consistent Modeling

The deformation textures of the compressed samples were calculated with the visco-plastic self-consistent polycrystal model (VPSC), developed by C.N. Tomé et al. [16]. In the model, each grain is treated as a visco-plastic ellipsoidal inclusion embedded in, and interacting with, a homogeneous effective medium that represents the aggregate [17]. Hardening and grain reorientations are accounted for. Twinned regions, which have a different orientation than the surrounding matrix, are treated as new grains with an evolving volume fraction [18]. As with slip,

twinning is assumed to have an associated CRSS for activation and hardening parameters. However, VPSC does not represent elastic deformation or the initial elastic-plastic transition. In this study, the model is used to help understand the effects of tensile twinning on the texture evolution with plastic strain, and to derive the activities of intrinsic deformation mechanisms that are difficult to determine experimentally.

The input data for the VPSC modeling is in three categories. The first is the boundary condition: the true plastic strain along the compression axis in this study. The second is the initial texture and grain shape that describe the polycrystalline Zircaloy-2 slab. These were taken from Ref. [19]. The last is the single crystal properties, consisting of thermal expansion coefficients, elastic constants and plastic deformation parameters. The thermal expansion coefficients and elastic constants are those reported in Ref. [19]. Plastic deformation parameters were adjusted so that the calculated flow curves fit best the experimental ones simultaneously for compression along three directions.

Four plastic deformation modes were considered: prismatic $\langle a \rangle$ slip $\{10\bar{1}0\}, 1/3\langle 11\bar{2}0 \rangle$ (pr), basal $\langle a \rangle$ slip $\{0001\}, 1/3\langle 11\bar{2}0 \rangle$ (bas), pyramidal $\langle c+a \rangle$ slip $\{10\bar{1}1\}, 1/3\langle 11\bar{2}3 \rangle$ (pyr) and tensile twinning $\{10\bar{1}2\}, \langle 10\bar{1}1 \rangle$ (tt). The evolution of CRSS for each mode is described by Voce hardening [20]. Table 1 lists the parameters used in the VPSC modeling. Tomé et al. [21] suggested that the hardening effects due to twin-slip (or twin-twin) interactions are stronger than those due to slip-slip interactions. Thus we used a higher ‘interaction hardening’ parameter concerning ‘twin-twin’ and ‘twin-slip’ interactions, i.e. $h^{slip-twin} = 2.0$, while we kept all $h^{slip-slip}$ as 1.0. Comparing the Voce-hardening parameters with those used in Ref. [12] for the EPSC modeling, we note that the relative initial CRSS’s of the slip and twinning modes are the same. Also the asymptotic hardening rate θ_1 for the slip modes are the same, while θ_1'' for VPSC modeling (0.40) is higher than that used for EPSC modeling (0.10). This difference is probably necessary because twinning is represented differently in VPSC than in EPSC. Specifically, EPSC does not account for the grain reorientations or texture development (which is much better treated in VPSC), thus a lower θ_1'' is needed in EPSC to generate softening commensurate with that brought about by the orientation changes associated with twinning in VPSC.

Table 1. Parameters describing the evolution of CRSS for each deformation mode: τ_0 and $\tau_0 + \tau_1$ are the initial and final back-extrapolated CRSS; θ_0 and θ_1 are the initial and asymptotic hardening rates.

	τ_0 (GPa)	τ_1 (GPa)	θ_0	θ_1
prism $\langle a \rangle$ slip	0.05	0.08	10.	0.02
basal $\langle a \rangle$ slip	0.08	0.08	10.	0.02
pyra. $\langle c+a \rangle$ slip	0.16	0.40	10.	0.40
tensile twinning	0.12	0.	0.40	0.40

4. Results and Discussion

4.1 Macroscopic stress-strain response

Although it is not sufficient, reproducing macroscopic stress-strain responses is the first important criterion for a successful model to reveal the texture evolution and the intrinsic deformation mechanisms. Figure 4 shows both the experimental and calculated macroscopic stress-strain behavior for compression along three directions. The experimental points in the figure represent the averaged stress and strain states where neutron diffraction measurements were performed. Clearly, the sample compressed along ND yields at a higher stress, and work-hardens more quickly than that compressed in TD and RD. The elastic-plastic transition is the most rapid during compression along RD, while it is relatively gradual along ND. Qualitatively reproducing the transition regions (as shown in Figure 4) by the model suggests that the CRSS ratio and the initial hardening rate of the deformation modes are reasonable, although the very sharp ‘corner’ at -0.5% strain in Figure 4c is not well captured. The starting points in the calculated curves do not

overlap the experimental ones, since the VPSC model is incapable of treating the elastic deformation, and the basic formula in the model do not allow for a ‘zero’ stress. It should be highlighted that the responses beyond -1.5% strain in each case are well predicted, especially for the compression along ND and along RD. In particular, the slight inflection of the experimental curve after -1.5% during compression along RD is well reproduced. This indicates that the values of the parameter used for the twinning (shown in Table 1) are in a reasonable range, since the inflection is caused by the initiation and hardening of tensile twinning [12]. In order to achieve reasonable values of the parameters, we stress the importance of achieving simultaneous agreement for the compression along all the three directions. Input values suitable for reproducing the response in only one or two directions do not guarantee the agreement in the other direction(s).

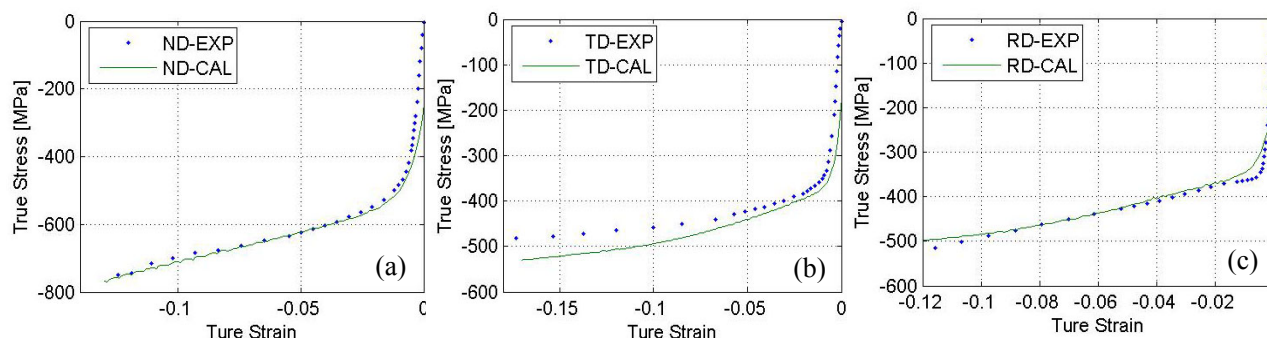


Figure 4. Experimental and calculated macroscopic stress-strain responses during (a) compression along ND, (b) compression along TD, and (c) compression along RD.

4.2 Measured texture development

The variation in intensity with strain was recorded for all the measured diffraction peaks in three directions. Here we present only the $\{10\bar{1}0\}$, $\{0002\}$ and $\{10\bar{1}1\}$ intensities during compression along RD. We reported the intensity changes of the prism and basal poles, for the compression along TD and RD in Ref. [13]. Here we briefly revisit them just in order to help understand the activation of twinning and to associate the intensity changes with the texture development.

Figure 5 shows the intensity changes with respect to the applied stress, for measurements taken in RD and ND, during compression along RD. Remarkable changes occur at -370MPa (or $\sim -1.7\%$ strain). Measured in RD, the initially absent $\{0002\}$ intensity increases dramatically above that stress, while the $\{10\bar{1}0\}$ and $\{10\bar{1}1\}$ intensities decrease in a significant rate. Measured in ND, the opposite is found for the prism and basal plane normals, i.e., the $\{0002\}$ intensity decreases while the $\{10\bar{1}0\}$ intensity increases. However, the $\{10\bar{1}1\}$ intensity also decreases in ND, but with a much smaller gradient. The opposite trend in intensity changes of the prism and basal poles shown in RD and ND is a clear signature of the occurrence of tensile twinning, since tensile twinning can bring about a $\sim 90^\circ$ reorientation of the prism and basal poles.

Ex-situ texture measurements have confirmed the activation of tensile twinning. As shown in the $\{0002\}$ pole figures (Figure 6b and 6e), after compression the $\{0002\}$ texture near ND is weaker, whereas the texture near RD is much stronger. The contours around ND in Figure 6e are skewed, which is probably caused by the buckling that occurred to the sample and/or the misalignment during texture measurement. Examining the prism pole figures (Figure 6a and 6d), it is easy to observe the decrease in the texture coefficient in RD, consistent with the intensity decrease observed in this direction during compression. After compression, the ‘1x random’ contour is much closer to ND, and the weakest texture has moved from the center to $\sim 30^\circ$ away from ND in the ND-RD plane. Thus it is reasonable to deduce that the prism texture is strengthened in ND after deformation, again consistent with the intensity changes observed in-situ. Changes in the $\{10\bar{1}1\}$ texture (Figure 7c and 7f) display the obvious decrease in the texture component in RD after compression. Around ND, the change in the texture component is too slight to discern, although it

can be considered to decrease since the random contour moves away from the center. Interestingly, distributions of the $\{10\bar{1}0\}$ and $\{10\bar{1}1\}$ texture components are very similar to each other after compression (Figure 6d and 6f).

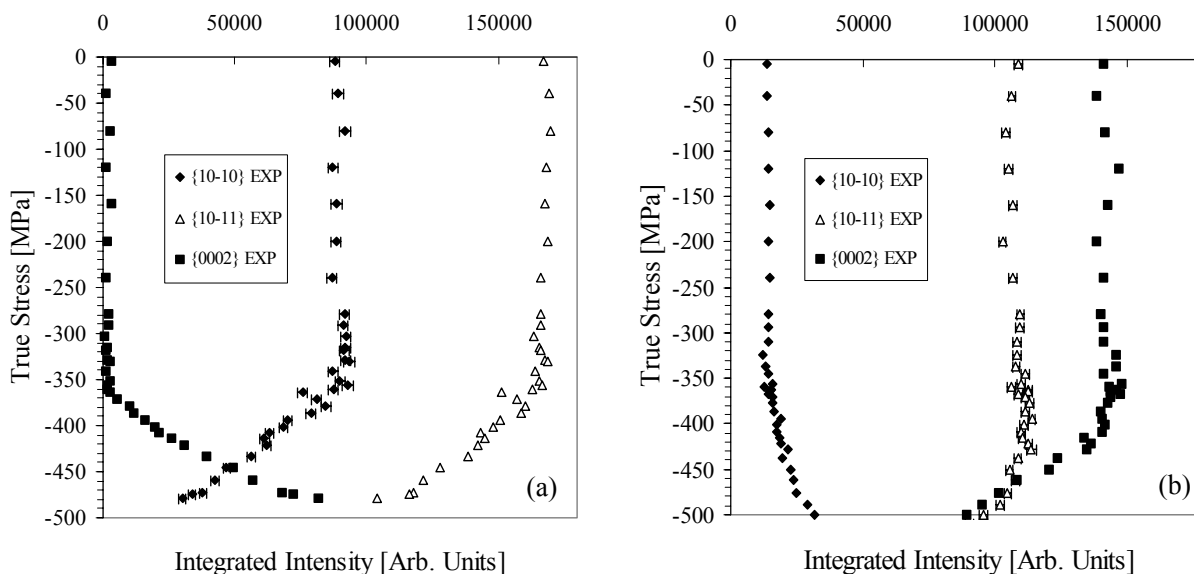


Figure 5. Intensity development for the $\{10\bar{1}0\}$, $\{0002\}$ and $\{10\bar{1}1\}$ reflections during compression along RD: (a) measured from RD, and (b) measured from ND. [13]

4.3 Predicted final texture

The calculated $\{10\bar{1}0\}$, $\{0002\}$ and $\{10\bar{1}1\}$ pole figures are shown in Figure 6g, 6h and 6i, respectively. From a qualitative point of view, the comparisons show good agreement with experimental measurements. Several similarities are shared by the predicted and measured $\{10\bar{1}0\}$ pole figures. Six strongest $\{10\bar{1}0\}$ texture lobes distribute at similar positions along the rim of the pole figures, while the weakest components are found around RD and in the “X”-shape region symmetrically aligned with respect to the center. The strongest and weakest $\{10\bar{1}1\}$ components show up at similar positions to those of the $\{10\bar{1}0\}$; however, the relatively highest strength is less than that of $\{10\bar{1}0\}$. The prediction again reasonably reproduced the $\{10\bar{1}1\}$ texture. As for the basal poles, clearly the predictions well reproduce their appearance around RD and also the propagation from ND to RD in the ND-RD plane. However, the increase in the intensity around RD is obviously over-predicted. Also, the calculated basal pole figure shows a split of basal poles near ND in the ND-RD plane, which was not clearly observed in the experiment.

Figure 7 presents the evolution of the relative activities of the three slip modes and tensile twinning. From the figure, the following deformation modes contribute to the strain in decreasing order of contribution: prism $\langle a \rangle$ slip, basal $\langle a \rangle$ slip and tensile twinning, at strains higher than -4%. Pyramidal $\langle c+a \rangle$ slip is nearly negligible (note that it is very active during compression along ND, however). The dominant activity of prism slip suggests that the deformation is mostly accommodated by this mode, which is consistent with the well-established fact that prism slip is the major mechanism during the deformation of zirconium and its alloys. Basal $\langle a \rangle$ slip also takes an important role in accommodating the plastic strain; it even accounts for more and more portion of the total activity as the deformation proceeds. Prism and basal slip may contribute to the formation of the six strong texture lobes on the rims of the $\{10\bar{1}0\}$ and $\{10\bar{1}1\}$ pole figures. As revealed by the modeling, significant tensile twinning takes place at approximately -1.0% strain; beyond that strain, its relative activity diminishes quickly. The predicted remarkable activation of tensile twinning corresponds to the small-range (from $\sim -1.0\%$ to $\sim -1.8\%$) saturation of the experimental stress-strain curve observed in Figure 4c. Thus we can deduce that the model does reasonably reproduce the occurrence of tensile twinning, although virtually it initiates a little earlier.

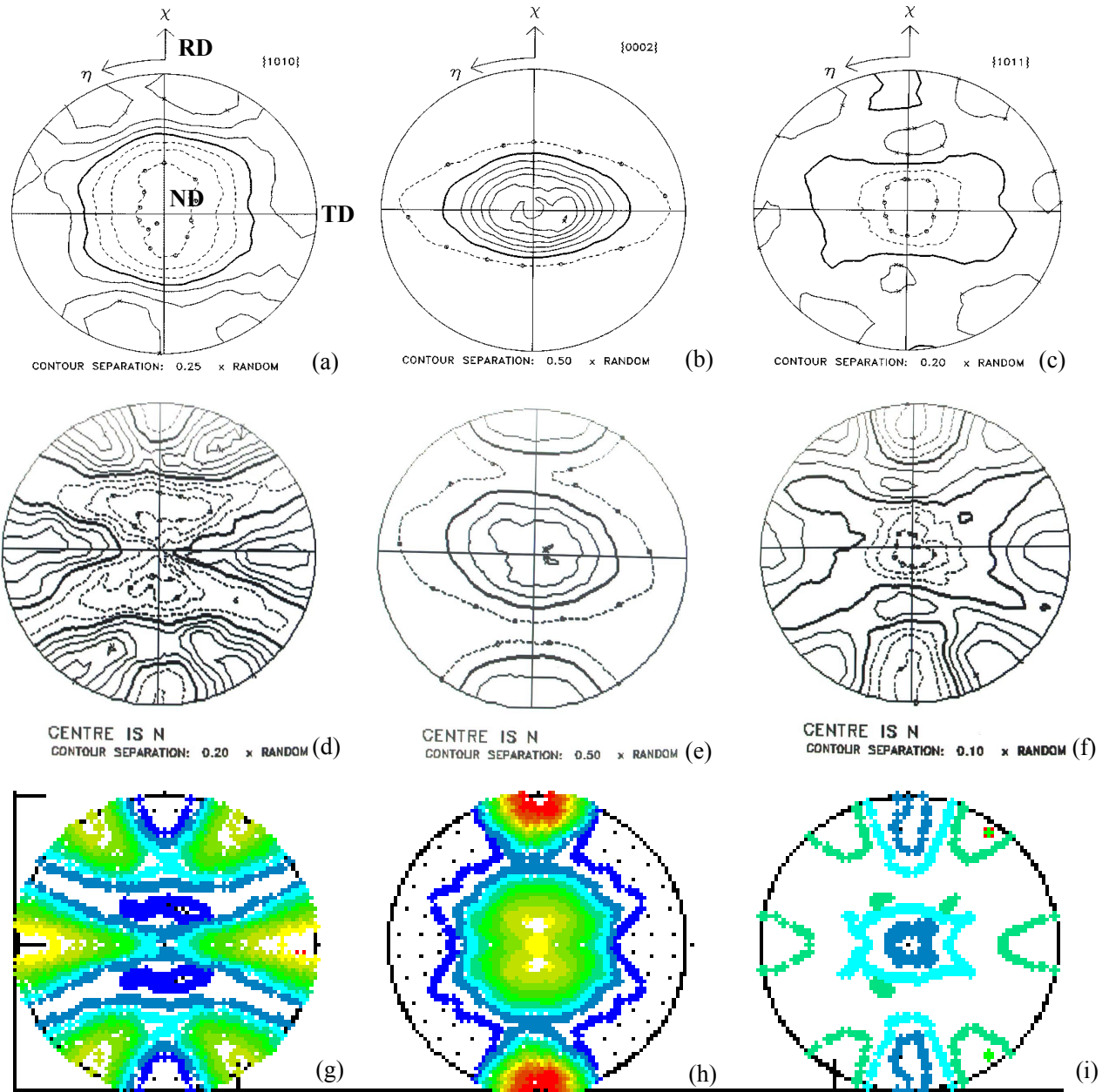


Figure 6. Measured and calculated pole figures: (a) measured initial $\{10\bar{1}0\}$ [14], (b) measured initial $\{0002\}$ [14], (c) measured initial $\{10\bar{1}1\}$ [14], (d) measured final $\{10\bar{1}0\}$, (e) measured final $\{0002\}$, (f) measured final $\{10\bar{1}1\}$, (g) calculated final $\{10\bar{1}0\}$, (h) calculated final $\{0002\}$ and (i) calculated final $\{10\bar{1}1\}$ (blue to red: low to high).

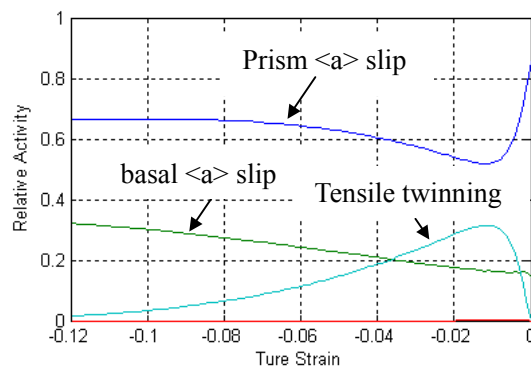


Figure 7. Evolution of relative activities of the deformation modes

5. Conclusion

Six in-situ compression tests have been performed along ND, TD and RD. The development of intensity was monitored in three principal directions during each test. The intensity changes during compression along RD indicated that significant tensile twinning occurred during the deformation. Textures of the deformed samples were then measured ex-situ at a different neutron site. The intensity changes of the basal pole, one prism pole and one pyramidal pole are consistent with the measured final texture. The measured basal pole figure confirmed the occurrence of tensile twinning which has brought about a portion of basal poles from ND to RD, and a portion of prism poles from RD to ND. Preliminary modeling work has been performed to reproduce the texture evolution. A visco-plastic self-consistent model was used and prism $\langle a \rangle$ slip, basal $\langle a \rangle$ slip, pyramidal $\langle c+a \rangle$ slip and tensile twinning were considered. The model qualitatively reproduced the macroscopic stress-strain responses and the final texture. As revealed by the modeling of the compression along RD, prism $\langle a \rangle$ slip is the leading deformation mechanism, while basal $\langle a \rangle$ slip and tensile twinning compete with each other as the next. Pyramidal $\langle c+a \rangle$ slip is negligible. In particular, the model discloses significant tensile twinning activities at a small strain during the deformation, which results in the accumulation of basal poles around RD. Further studies are needed to quantify the volume fraction of tensile twinning, both experimentally and theoretically.

Acknowledgements

Feng Xu thanks Dr. C.N. Tomé of LANL for providing VPSC6 for our calculations and POLE7 for the data analysis. This work is sponsored by NSERC, COG, OPG and Nu-Tech Precision Metals under the Industrial Research Chair Program in Nuclear Materials at Queen's University.

References

- [1] S.R. MacEwen, J. Faber and A.P.L. Turner, *Acta Metall.* 31 (1983) 657-676.
- [2] Canada Enters the Nuclear Age, Atomic Energy of Canada Limited (1997).
- [3] J. Hopwood, Proc. 26th Annual Conference of the Canadian Nuclear Society, paper P23, 2005.
- [4] A. Akhtar, *Acta. Metallurgica* 21 (1973) 1-11.
- [5] H.R. Wenk, *J. Appl. Cryst.* 31 (1998) 262.
- [6] J.W.L. Pang, T.M. Holden, P.A. Turner, and T.E. Mason, *Acta Mater.* 47 (1999) 373-383.
- [7] R.G. Ballinger and R.M. Pelloux, *J. Nucl. Mater.* 97 (1981) 231-253.
- [8] R.G. Ballinger, G.E. Lucas and R.M. Pelloux, *J. Nucl. Mater.* 126 (1984) 53-69.
- [9] Hobson, D.O., *Transactions, The Metallurgical Society, American Institute of Mining, Metallurgical and Petroleum Engineers*, Vol. 242 (1968) 1105.
- [10] Erich Tenckhoff, *Deformation mechanisms, texture and anisotropy in zirconium and zircaloy*, ASTM special technical publication; 966 (1998).
- [11] S.R. Agnew, M.H. Yoo and C.N. Tomé, *Acta mater.* 49 (2001) 4277-4289.
- [12] F. Xu, R.A. Holt and M.R. Daymond, (*in preparation*).
- [13] F. Xu, R.A. Holt, E.C. Oliver and M.R. Daymond, (*submitted to Proc. MecaSens 2005*).
- [14] R.A. Holt, D. Dye, R.B. Rogge, Annual Report of the National Research Council (2004)
- [15] Larson, A.C and Von Dreele, R.B. (1994) General Structure Analysis System, Report No. LAUR 86-748.
- [16] C.N. Tomé, P.J. Maudlin, R.A. Lebensohn, and G.C. Kaschner, *Acta mater.* 49 (2001), 3085-3096.
- [17] D.W. Brown, S.R. Agnew et al., *Materials Science and Engineering A* 399 (2005) 1-12
- [18] P. Rangaswamy, M.A.M. Bourke, et al., *Metallurgical and Materials Transactions* 33A (2002) 757-763.
- [19] F. Xu, R.A. Holt, R.B. Rogge and M.R. Daymond, *Proc. CNS-26*, 2005.
- [20] P.A. Turner and C.N. Tomé, *Acta Metall.* 42 (1994) 4143-4153
- [21] C.N. Tomé, P.J. Maudlin et al., 49 (2001) 3085-3096.